Real-Time Simulation of Heat Transfer in Continuous Casting

SEPPO LOUHENKILPI, ERKKI LAITINEN, and RISTO NIEMINEN

A real-time heat-transfer model for continuous slab casting is presented. The model calculates the strand temperatures and the solid shell thickness profile along the machine as a function of the actual casting variables, strand geometry, and steel grade. The special requirements concerning the real-time use of the model and, in general, the accuracy of the model are also studied and discussed. The model has been tested by carrying out industrial trials. Some examples of the differences between the calculated and measured surface temperatures are presented. A special procedure to determine the boundary conditions for the secondary cooling zones from temperature measurements is also described.

I. INTRODUCTION

THE careful control of the strand cooling and the shell growth along the machine is of central importance in continuous casting operation. These have a considerable influence on the formation of cracks and other defects which can be formed in the cast material. To ensure defect-free products, the strand is to be cooled down according to a pattern which depends on steel grade, product dimension, casting speed, and machine design. On the other hand, the control of the liquid pool length is a key element in optimizing the casting speed with respect to good productivity. So, the heat transfer plays a very important role in continuous casting, especially when casting crack-sensitive steel grades.

To study the thermal state of a continuously cast strand, two methods can be used: empirical correlation of numerous experimental results and mathematical simulation models supported by experimental results. It is difficult and inaccurate to measure, at least inside the spray chamber, the strand temperatures or the shell thickness during casting. Moreover, the empirical models cannot be used to extrapolate the results outside the experimental range and generally they cannot be used for simulation of transient casting conditions. Mathematical models, on the other hand, once verified are easy to use and comprehensive in simulating the thermal state of the strand.

In recent years, many mathematical heat-transfer models for continuous casting have been developed.[1-21] However, most of the models can be used only for simulation of steady state casting operations in off-line. They give the strand temperature field as a function of casting parameters, such as the casting speed, superheat, mold heat removal, spray water flow rates, steel grade, and strand geometry. The numerical approximation of the model is usually done by the finite difference or finite element method. Heat-transfer models are being increasingly used to improve the existing cooling systems, to improve casting practices, and for process control.

SEPPO LOUHENKILPI, Senior Teaching Assistant, is with the Laboratory of Metallurgy, Helsinki University of Technology, 02150 Espoo. Finland. ERKKI LAITINEN, Associate Professor, and RISTO NIEMINEN, Researcher, are with the Department of Mathematics, Jyväskylä University, 40100 Jyväskylä, Finland.

Manuscript submitted October 13, 1992.

Although the steady state models offer important knowledge for the operational limits of the continuous casting machine, they are not valid for simulation of transient casting conditions which occur rather frequently. For better control of heat transfer over the whole continuous casting cycle, more attention has recently focused on developing real-time simulation models which are valid under transient casting conditions.[16-21]

In the real-time simulation, many practical requirements will be set for the simulation model. The computing time must, for instance, be short enough and the special process conditions, such as the start and the end of casting, must be included in the model.

In the present article, a real-time heat-transfer model for continuous casting is presented. The model calculates the strand temperature field in a longitudinal cross section through the middle of the strand. The longitudinal heat conduction is taken into account; therefore, the model can be applied also for the simulation of continuous casting of copper, aluminum, and other metals where this factor is significant. The numerical approximation of the heat-transfer model is based on the finite element method.

For the correct simulation of heat transfer in continuous casting, the determination of the boundary conditions describing the heat-transfer phenomena through the strand surface is of crucial importance. The boundary conditions are usually expressed as heat fluxes or heat-transfer coefficients. A procedure to determine the boundary conditions for the secondary cooling zones from the temperature measurements is presented in this article.

For the validation of the heat-transfer model, a lot of strand surface temperature measurements were carried out on a slab casting machine and the measured temperatures were compared with the calculated ones. The special requirements concerning the real-time use of the model and, in general, the accuracy of the model are also studied and discussed.

II. THE REAL-TIME SIMULATION MODEL

The model simulates the temperature field in a longitudinal cross section through the middle of the strand. The calculation domain is schematically shown in Figure 1. The model is two- dimensional (2-D), the dimensions being the casting direction and the direction

perpendicular to the wide face of the strand. The heat flow along the width direction of the strand is neglected. In the case of rectangular sections, such as slabs and thin sections, this simplification is generally accepted, but for blooms or billets, the model cannot be directly applied. The other typical assumptions made in the model are that (a) the solidus and liquidus temperatures as well as other phase transformation temperatures are constant, (b) the solidification takes place by directional dendritic growth, (c) the material behavior is isotropic, and (d) the cooling is symmetrical on the top and bottom sides of the slab. These assumptions are generally made also in steady state models.

Heat transfer within this 2-D domain can be mathematically defined by

$$\frac{\partial H(T)}{\partial t} + v(t)\frac{\partial H(T)}{\partial y} = \nabla \cdot (k(T)\nabla T) \qquad [1]$$

where H is the enthalpy, t is time, k is thermal conductivity, T is temperature, and v is the actual casting speed. Enthalpy H is defined as the sum of sensible and latent heats:

$$H(T) = \Delta h(T) + \Delta H(T) \qquad [2]$$

where the sensible heat, $\Delta h(T)$, and the latent heat, $\Delta H(T)$, are defined as

$$\Delta h(T) = \rho \int_0^T c(\Theta)\, d\Theta \qquad [3]$$

and

$$\Delta H(T) = \rho L \int_0^T -\frac{\partial f_s}{\partial \Theta}\, d\Theta = \rho L\,(1 - f_s(T)) \qquad [4]$$

where ρ is density, c is specific heat, L is latent heat, and $f_s = f_s(T)$ is solid fraction. The solid fraction describes the manner in which the latent heat is released between the solidus and liquidus temperatures. This manner is very sensitive to the chemical composition of the metal being cast and is not always known accurately. The effect of the form of f_s on the calculated results is described in Section VI. If there are other phase transformations in the solid state, such as the Δ-ferrite to austenite and the austenite to α-ferrite, they can be taken into account in a similar way.

Applying Kirchhoff's transformation,

$$K(T) = \int_0^T k d\Theta \qquad [5]$$

Eq. [1] becomes:

$$\frac{\partial H}{\partial t} = \frac{\partial^2 K}{\partial x^2} + \frac{\partial^2 K}{\partial y^2} - v\frac{\partial H}{\partial y} \qquad [6]$$

The last term in Eq. [6] represents the convective heat transfer due to the movement of the strand.

The convective heat transfer in the liquid due to the fluid flow is difficult to calculate using differential equations. The technique most often used to account for the convective heat transfer is effective thermal conductivity.[11,22,23] This technique is also used in the present case. The effective thermal conductivity is approximated by the following linear relationship:

$$k_{\text{eff}}(T) = k(T) f_s + Ak(T)\,(1 - f_s) \qquad [7]$$

where k is thermal conductivity and A is a parameter.

If the parameter A is 1, there is no increased heat transfer in the mushy or liquid regions due to the fluid flow. Figures 2 and 3 show calculated shell thicknesses and slab surface temperatures with $A = 1$ and $A = 5$. The parameter A has more influence on the results within the liquid pool than in the solid shell. Normally, a value of 5 is used in our calculations. Mizikar[22] reported that the empirical k_{eff} was roughly 7 times greater than the liquid thermal conductivity, and this approach is generally used in solidification simulations. However, Mizikar used the effective thermal conductivity only over the region where the temperatures were over the liquidus temperature. In the present model, the effective thermal conductivity is used also over the mushy region, *i.e.*,

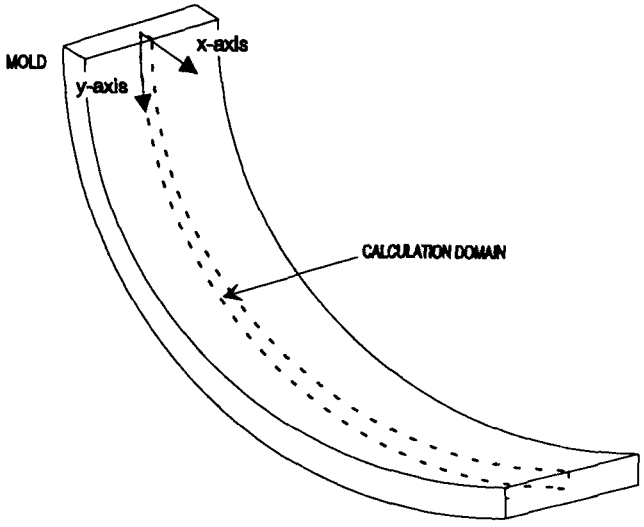

Fig. 1—The calculation domain schematically presented.

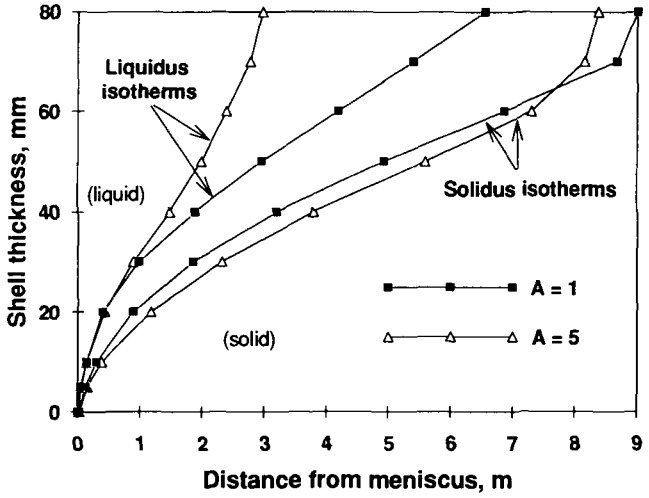

Fig. 2—Solidus and liquidus isotherms calculated with $A = 1$ and $A = 5$ (T_0 = 1500 °C, T_L = 1454 °C, and T_S = 1399 °C).

where the temperature is between the liquidus and solidus temperatures (Eq. [7]). That is the reason why a little smaller value of constant A is used in our calculations.

III. BOUNDARY AND INITIAL CONDITIONS

In order to solve Eq. [6], the following boundary and initial conditions are used.

(1) During steady casting, the liquid surface at the top of the mold is the upper boundary of the calculation domain. Here, the temperature is assumed to be equal to the incoming liquid temperature $T_0 = T_0(t)$. Hence,

$$T(x, 0) = T_0 \qquad [8]$$

During the end of the cast, this boundary descents with the strand according to the actual casting speed and radiative heat flux is used as a boundary condition. Thus,

$$-k\frac{\partial T}{\partial n} = \sigma\varepsilon(T^4 - T_{ext}^4) \text{ during the end of the cast} \qquad [9]$$

(2) The convective energy transport due to the strand movement, $Q = Q(x; t)$, is used as the boundary condition at the lower boundary of the domain:

$$Q = vH \qquad [10]$$

(3) At the strand surface along the mold length, the heat flux through the mold wall, $Q = Q(y; t)$, is used as a boundary condition. The average heat flux, Q_{ave}, extracted from the mold is calculated from the heat balance of the mold cooling water:

$$Q_{ave} = \rho_w c_w W\frac{\Delta T}{A_m} \qquad [11]$$

Here, ΔT is the temperature increase of the mold cooling water, A_m the area of the mold face, and W the cooling water flow rate. The heat flux distribution along the mold length, Q, is then calculated by fitting the average heat flux to experimentally obtained heat flux profiles.[6,24,25] Hence, the heat flux through the mold wall can be expressed as

$$-k\frac{\partial T}{\partial n} = Q \qquad [12]$$

The total amount of heat flux can be easily measured, but the heat flux profile varies with casting parameters, *e.g.*, with casting speed and the steel grade to be cast. However, this profile is not always very well known.

To investigate how sensitive the simulation model is to the changes of the mold heat flux profile, test calculations were carried out. Strand surface temperatures calculated with two different mold heat flux profiles are presented in Figure 4. The total amount of the mold heat flux, Q_{ave}, was the same. In the fitted case (Figure 4), the air gap formation was approximated by decreasing the heat flux at the bottom of the mold. In the unfitted case, the heat flux was distributed uniformly along the mold. As can be seen (Figure 4), the different approximation of the heat flux distribution profile has a minor effect on the temperatures in the solid shell below the mold. Inside the mold, however, the influence is considerable. So, the correct assignment of the mold heat flux distribution profile is important only when studying temperatures in the mold region or immediately below it.

(4) At the strand surface below the mold, the heat flux from the strand surface to the environment takes place by a combination of the three heat-transfer mechanisms: conduction, convection, and radiation. It is very difficult to determine the shares of each mechanism on the total heat transfer. In the present model, an effective heat-transfer coefficient, h, is used. This takes into account the total heat transfer except the radiation. Hence, the boundary condition is

$$-k\frac{\partial T}{\partial n} = h(T - T_w) + \sigma\varepsilon(T^4 - T_{ext}^4) \qquad [13]$$

The last term represents the heat flux by radiation. Before this boundary condition can be applied in industrial computations, the relationship between the effective heat-transfer coefficient and the cooling parameters, *e.g.*, spray water flow rates, strand surface temperatures, *etc.*, must be determined for each cooling zone. Approximate values can be found in the literature,[7–10,26–28] but for a specific caster and steel grade, these can be determined more precisely on the basis of surface temperature measurements, for instance, using pyrometers or thermoelements. This can be done by using, for instance, a method which is presented in Section VII.

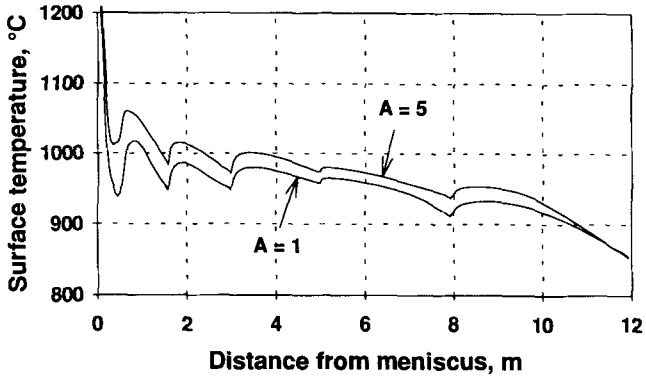

Fig. 3—Strand surface temperature profile calculated with $A = 1$ and $A = 5$ ($T_0 = 1500$ °C, $T_L = 1454$ °C, and $T_S = 1399$ °C).

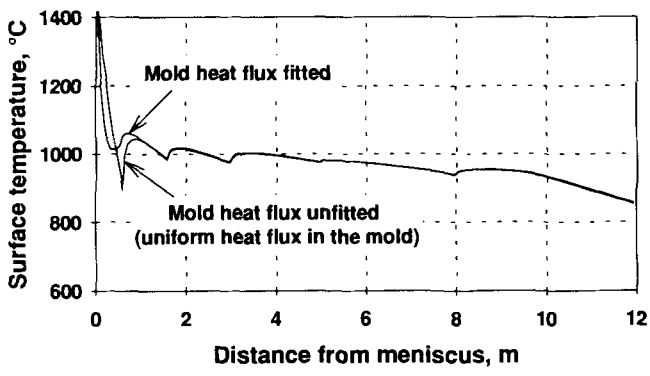

Fig. 4—Strand surface temperatures for uniform (=unfitted) and for nonuniform (=fitted) heat flux from the mold.

If local variations in the temperature distribution within a cooling zone are of interest, the effective heat-transfer coefficient must be determined locally in more detail.

(5) Because the cooling is assumed to be equal on the top and bottom surfaces, there is no heat flux through the centerline of the slab. Hence, the boundary condition through the centerline is

$$-k\frac{\partial T}{\partial n} = 0 \qquad [14]$$

The initial condition at the time $t = 0$ is defined as

$$T(x, y) = \begin{cases} T_0, & y = 0 \\ T_{\text{start}}, & y > 0 \end{cases} \qquad [15]$$

where T_{start} is a given temperature without any physical importance.

Equations [6] through [15] are solved numerically using the finite element method in space and finite difference method in time. In the finite element method, the partial differential equations to be solved are first transformed to algebraic matrix equations. They are then solved using iterative matrix solution methods. The solution of the finite element matrix equation gives the unknown temperatures at nodal points.

IV. NUMERICAL SOLUTION OF THE MODEL EQUATIONS

In the present work, standard triangle elements with linear shape functions are used. The following finite element matrix equation results from the standard piecewise linear space discretization of Eqs. [6] through [15]:

$$[M]\frac{\partial \mathbf{H}}{\partial t} + [C]\mathbf{H} + [A]\mathbf{K} + [B]T = F \qquad [16]$$

where $[M]$ = mass matrix;
$[C]$ = convection matrix;
$[A]$ = stiffness matrix;
$[B]$ = boundary condition matrix;
$\mathbf{F}$ = load vector;
$\mathbf{T} = (T_1, T_2, \ldots, T_n)$ = temperature vector;
$\mathbf{K} = (K(T_1), K(T_2), \ldots, K(T_n))$ = Kirchoff's transform vector; and
$\mathbf{H} = (H(T_1), H(T_2), \ldots, H(T_n))$ = enthalpy vector.

For time discretization, it is denoted

$$\frac{\partial \mathbf{H}}{\partial t} \approx \frac{\mathbf{H}^{i+1} - \mathbf{H}^i}{\Delta t} \qquad [17]$$

where the superscripts i and $i + 1$ refer to time events $t = t^i$ and $t = t^{i+1}$, respectively, and Δt is the time step between t^i and t^{i+1}. By applying an implicit finite difference scheme, Eq. [16] can be rewritten as

$$\frac{[M]}{\Delta t}\mathbf{H}^{i+1} + [C]\mathbf{H}^{i+1} + [A]\mathbf{K}^{i+1} + [B]T^{i+1} = F^{i+1} + \frac{[M]}{\Delta t}\mathbf{H}^i \qquad [18]$$

An implicit finite difference scheme is used, because the explicit method places much stricter requirements on the time step size. However, the normal piecewise linear finite element approximation, as in Eq. [18], becomes unstable when[29]

$$\text{Pe} = \frac{\rho c|v|d}{k} > 2 \qquad [19]$$

where Pe = discrete Peclet number;
ρ = density;
v = fluid velocity;
d = element size; and
k = thermal conductivity.

Equation [19] indicates that the size of finite elements must be small if the casting speed is large. In the case of continuous casting, this condition leads, in general, to a very refined element model and, hence, to high computing times. It is very difficult to fulfill this condition in real-time simulation, because the calculation cycle must be short. One method to overcome this is the upwind method.

The essential point of the upwind technique is the additional term of artificial conductivity in the convection term. The form of this term depends on the velocity, specific heat, and the element size of the finite element model. In the case of continuous casting, the artificial conductivity may be added along the casting direction. The additional artificial conductivity k^{ac} is defined by[29]

$$k^{ac} = \alpha\frac{1}{3}(\rho c v d) \qquad [20]$$

where α is the parameter ($0 \le \alpha \le 1$).

The representative element size d is, in the case of triangular elements, the length of the longest side of the element. If the parameter α is 0, then no artificial conductivity is applied.

Now Eq. [18] can be modified by adding the artificial conductivity term into the convection term:

$$\frac{[M]}{\Delta t}\mathbf{H}^{i+1} + ([C] + [A^{ac}])\mathbf{H}^{i+1} + [A]\mathbf{K}^{i+1} + [B]T^{i+1} = F^{i+1} + \frac{[M]}{\Delta t}\mathbf{H}^i \qquad [21]$$

where $[A^{ac}]$ is the artificial conduction matrix.

More details on the upwind method can be found in References 29 through 31. Equation [21] is now the discretized model equation. It is solved for temperature using iterative methods. Details of the solution methods are given in References 32 through 34.

V. ON THE SPEED OF THE NUMERICAL SOLUTION ALGORITHM

The accuracy of the numerical solution depends mainly on the FE-discretization of the domain. The solutions are comparatively independent of the choice of the discretization as long as the FE-discretization parameters are

sufficiently small. The FE-element mesh used also influences the calculation time which, in real-time simulation, must be short. The Fe-mesh size is a compromise between the accuracy of the solution and calculation time.

For testing purposes, the simulation model was solved on a microcomputer and two transputer processors in parallel by using the pipeline technique.[35] The simulation program runs on the two transputer processors on a motherboard plugged into the microcomputer, while the user interface of the program runs simultaneously on the micro's own processor under the Windows environment.

In order to study the effects of the time step size and the convergence criterion on the computing time, test trials were carried out. In the test cases, the length of the calculation domain was chosen to be 20.0 m the thickness to be 85 mm. The FE-mesh size was, on average, 10 mm in the thickness direction and 50 to 200 mm in the longitudinal direction, and the total number of nodes was 1540.

In Figure 5, a so-called relative computing time is presented as a function of time step. In real-time simulation, the relative computing time (absolute computing time/length of time step) must be much smaller than 1. For instance, using a 5 second time step, the relative computing time is about 0.4, which means that the absolute computing time is about 2 seconds. When the time step becomes shorter, the absolute computing time becomes shorter also, because the changes in temperature variations between time steps decrease. However, the computing time decreases less than the time step, and thus, the relative computing time increases. In a normal continuous casting machine, a calculation cycle of 5 seconds is believed to be short enough. This can be fulfilled quite easily with the presented installation. The convergence criterion of 0.2°C was used in these trials. Figure 6 shows the relation between the number of iterations and the convergence criterion.

VI. MATERIAL PROPERTIES

For thermophysical properties, such as thermal conductivity, $k(T)$, specific heat, $c(T)$, density, $\rho(T)$, latent heat, L, and solid fraction, $f_s(T)$, necessary for the simulation, literature data were used.[36,37,38]

However, it is not always possible to find all the data for a steel grade close enough to the chemical composition to be cast. This is especially the case for $f_s(T)$ which can be a strong function of temperature. Test calculations with linear and nonlinear shapes of f_s were carried out to study the effect of f_s on the calculation results. Figure 7 presents some results. The shape does not affect the results in the solid shell significantly but has more influence on the results in the liquid pool. In the nonlinear case, f_s was calculated by the computer program developed by Miettinen.[39] The steel grade used was AISI 304L. The nonlinear solid fraction calculated is presented in Figure 8. Normally, a nonlinear f_s is used in our calculations.

VII. DETERMINATION OF HEAT-TRANSFER COEFFICIENTS FOR THE SPRAY COOLING ZONES

In the case of normal spray water cooling, the heat-transfer coefficient depends mainly on the spray water

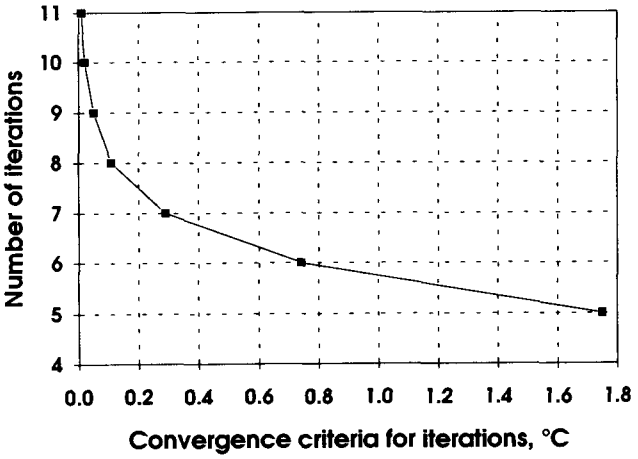

Fig. 6—An example of dependence of number of iterations on convergence criterion (time step, 5 s).

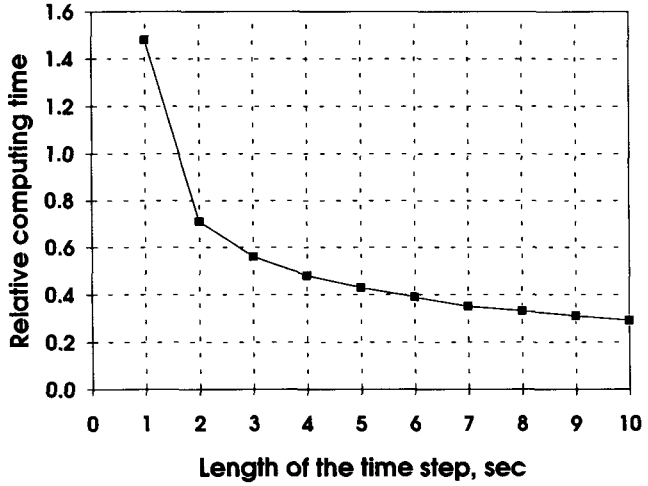

Fig. 5—An example of dependence of relative computing time on length of time step (convergence criterion, 0.2 °C).

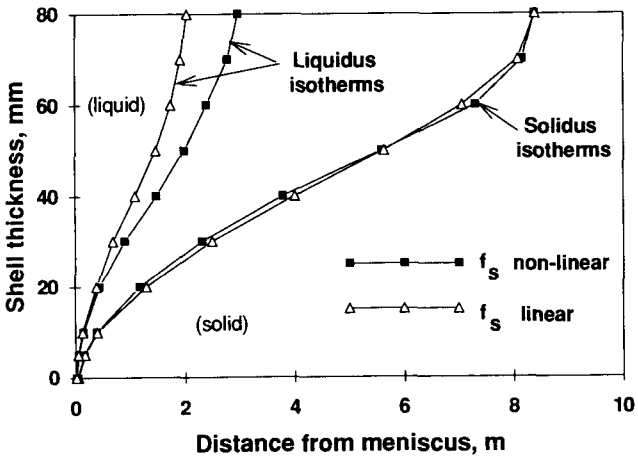

Fig. 7—Solidus and liquidus isotherms calculated with linear and nonlinear shapes of f_s. The nonlinear shape is calculated for AISI 304L (Fig. 8).

flow rate and on the surface temperature of the strand. Before the developed heat-transfer model can be applied in industrial computations, the relationship between the heat-transfer coefficient and the spray cooling parameters must be determined separately for each cooling zone.

In the present work, empirical formulas for the heat-transfer coefficient were derived for a slab casting machine. The caster was of curved type with a straight mold, and the secondary cooling consisted of five zones with normal water spray cooling. The strand temperatures were measured with pyrometers under steady and unsteady state casting conditions. Infrared pyrometers were located at 2.7 and 5.8 m below the mold. The temperature was also measured near the straightening unit. The measurements were carried out on both the bottom and top sides of the strand. For other sections of the strand, empirical formulas were estimated from the literature.

The following equations were used to describe the relationship between the heat-transfer coefficients, the spray water, and the slab surface temperature:

$$h_i = \begin{cases} (\alpha_i W_i + \beta_i)\gamma_i(T) & W_i > 60 \dfrac{l}{\mathrm{m^2\ min}}, \text{ (zones 1 and 2)} \\ \alpha_i W_i^{\beta_i}\gamma_i(T) & W_i \le 60 \dfrac{l}{\mathrm{m^2\ min}}, \text{ (zones 3 and 4)} \end{cases} \quad [22]$$

Here α_i, β_i, and γ_i are parameters for zone i. The parameter γ_i is a function of temperature, and it takes into account the effect of the strand surface temperature on the heat-transfer coefficient. The strand surface temperature has little effect on h when it is higher than the Leidenfrost temperature and the parameter $\gamma_i = \gamma_i(T)$ is set equal to one.

The parameters α_i, β_i, and γ_i were derived in two steps. In the first step, α_i and β_i were derived from measurements done under conditions in which γ_i could be set equal to 1. In the second step, for temperatures below the Leidenfrost temperature, γ_i was derived using values determined in step 1 for α_i and β_i.

These two steps are described subsequently.

Step 1

(1) Assume that the process is under steady state at time $t = t^0$. Change the water flow rates during a time period (t^0, t^n). For time events $t^0 < t^1 < \ldots < t^n$, measure data about surface temperatures, superheat, casting speed, mold heat flux, and spray water flow rates.

(2) Set time index $k = 0$.

(3) Increase the time by setting $k = k + 1$. Set initial guess for the heat-transfer coefficient $h_i = h^k$.

(4) Input the at time t^k measured process data to the developed simulation model and calculate the surface temperature at time t^k.

(5) IF the calculated temperature does not match the measured temperature, THEN change the heat-transfer coefficient h_i slightly and goto (4), ELSE save h_i and W_i at time t^k.

(6) If $k < n$ goto (3) (new time step begin).

(7) Apply a standard curve fitting method for solving the parameters α_i and β_i from Eq. [22] using the calculated time series of $(h_i(t^1), \ldots, h_i(t^n))$ and measured time series of $(W_i(t^1), \ldots, W_i(t^n))$

This simulation procedure is generally repeated separately for each zone where measurements are taken, starting from the zone nearest to the mold. This is because the parameters for the previous zones must always be known. The flow chart is shown in Figure 9.

Step 2

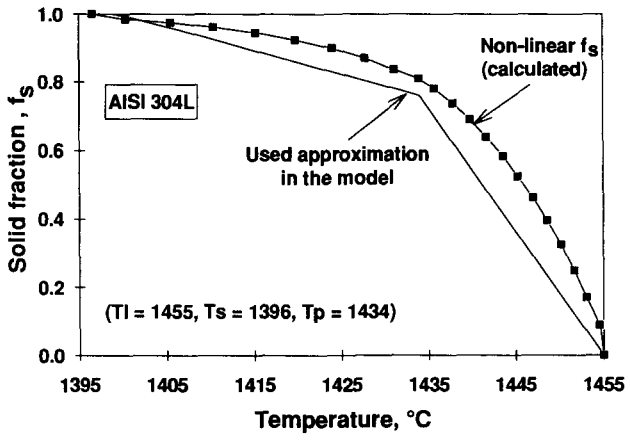

Fig. 8—Solid fraction *vs* temperature during solidification for AISI 304L calculated by the solidification model.[39]

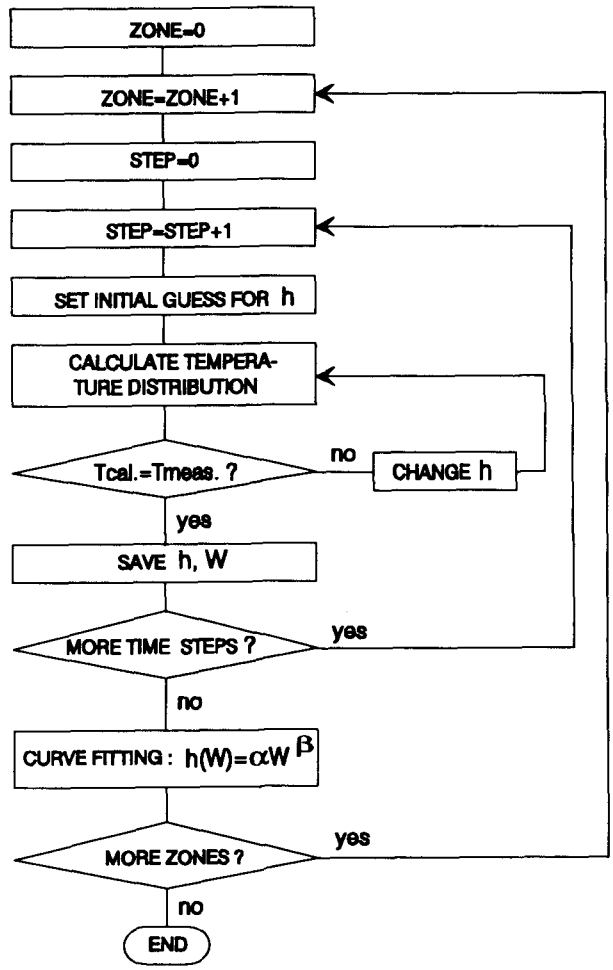

Fig. 9—Flow chart showing the determination of the parameters α_i and β_i in the correlation $h_i = \alpha_i W_i^{\beta_i}$ or $h_i = \alpha_i W_i + \beta_i$.

In this step, the parameter $\gamma_i(T)$ was determined experimentally by fitting the calculated temperatures to the measured ones. During these measurements, the spray water flow rates were kept constant but the casting speed was changed so that the strand surface temperature fell below the Leidenfrost temperature. The parameters α_i and β_i were the same are were derived beforehand in step 1.

Figure 10 shows the variation of γ with temperature. In our test calculations, this was used for each zone. The parameters α_i and β_i obtained in step 1 are presented in Section VIII.

VIII. COMPARISON OF CALCULATED RESULTS WITH MEASURED VALUES

To test the accuracy of the model, surface temperatures measured with pyrometers were compared with the calculated values obtained by the model. The measurements were performed with a stainless steel slab caster.

Some results between the surface temperature calculated by the model and measured by the pyrometers are shown in the Figures 11 through 13. The pyrometer data presented are 15-second mean values of the measured 1-second temperatures. It is assumed that the fluctuations in surface temperature are caused by the scale on the surface of the slab, and the top temperatures are near the actual surface temperatures.

In Figure 11, the temperatures in zone 3 at 2.7 m below the mold on the bottom side of the strand are compared. The steel grade was AISI 304L. The following correlation was used for the heat-transfer coefficient for the zones $i = 1$, 2, and 3:

$$h_i = \begin{cases} 0.019\, W_i^{0.74}\, \gamma(T) & W_i \le 60 \dfrac{l}{\text{m}^2\,\text{min}} \\ (0.003\, W_i + 0.21)\, \gamma(T) & W_i > 60 \dfrac{l}{\text{m}^2\,\text{min}} \end{cases} \quad [23]$$

The casting speed was changed during this trial, but the water flow rates were constant. As Figure 11 shows, quite a good agreement between the calculated and measured values is obtained.

In Figure 12, the comparison point is the same as in Figure 11 but now on the top side of the strand. The steel grade was AISI 321. The correlation for the heat-transfer coefficient for the zones $i = 1$, 2, and 3 was now the following:

$$h_i = \begin{cases} 0.0175\, W_i^{0.74}\, \gamma(T) & W_i \le 60 \dfrac{l}{\text{m}^2\,\text{min}} \\ (0.003\, W_i + 0.18)\, \gamma(T) & W_i > 60 \dfrac{l}{\text{m}^2\,\text{min}} \end{cases} \quad [24]$$

The casting speed was kept constant during this trial except at the end of the casting, but the water flow rates were increased suddenly by 40 pct during the casting (Figure 12). Quite good agreement between the calculated and measured results is again obtained.

In Figure 13, the comparison point is in zone 4, 5.8 m below the mold on the bottom side of the strand. The steel grade was AISI 316L. Equation [23] was used for the first three zones, but for the fourth zone, the following correlation was used:

$$h_4 = \begin{cases} 0.021\, W_4^{0.74}\, \gamma(T) & W_4 \le 60 \dfrac{l}{\text{m}^2\,\text{min}} \\ (0.003\, W_4 + 0.25)\, \gamma(T) & W_4 > 60 \dfrac{l}{\text{m}^2\,\text{min}} \end{cases} \quad [25]$$

In this case, the strand surface temperature is quite low and there are high fluctuations in the measured temperature. It is difficult to know if the fluctuation is a measurement error or not. Error could be caused, for instance, due to scale on the surface of the slab. Our opinion is that the fluctuation is caused due to the error in measurements (scale), and the top temperatures are close to the actual surface temperatures. So, the agreement between the results is again quite good.

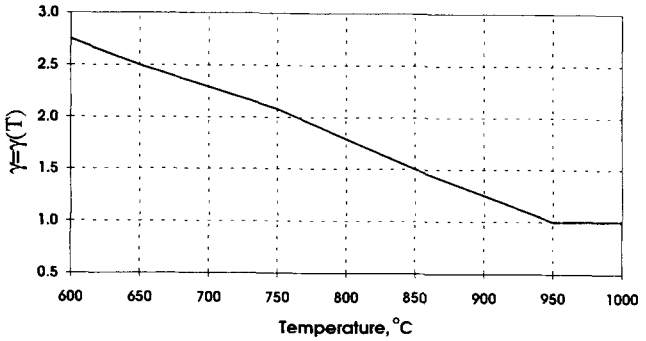

Fig. 10—The parameter $\gamma(T)$ obtained from the measurements.

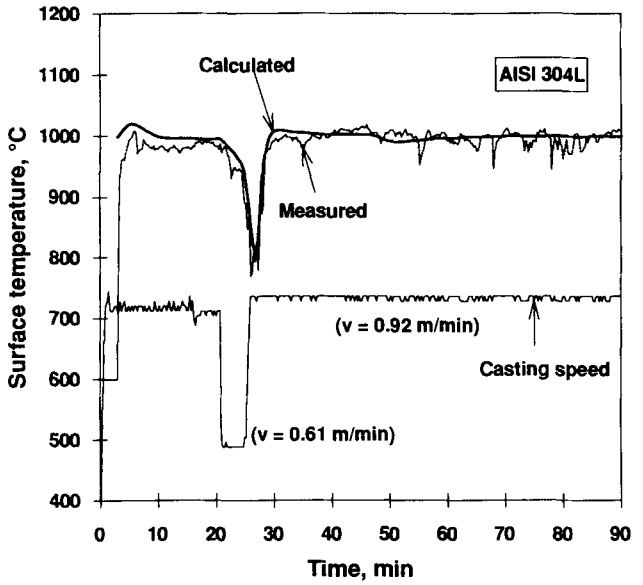

Fig. 11—Comparison between calculated and measured surface temperatures for steel grade AISI 304L with change in casting speed. The comparison point is 2.7 m below the mold on the bottom side.

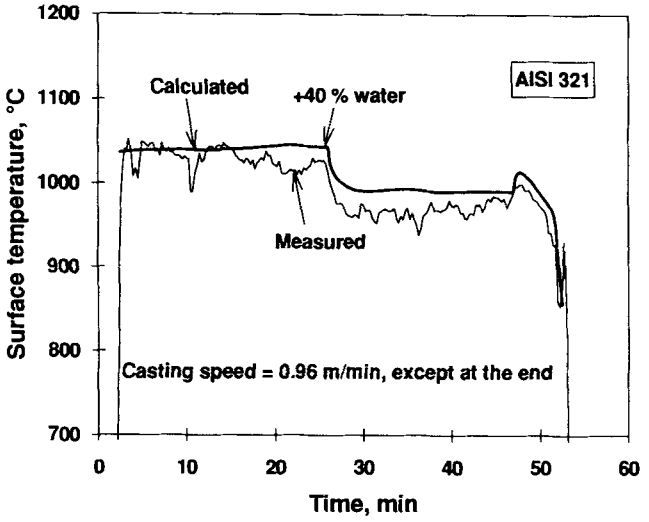

Fig. 12—Comparison between calculated and measured surface temperatures for the steel grade AISI 321 with change in the spray water flow rates. The comparison point is 2.7 m below the mold on the top side.

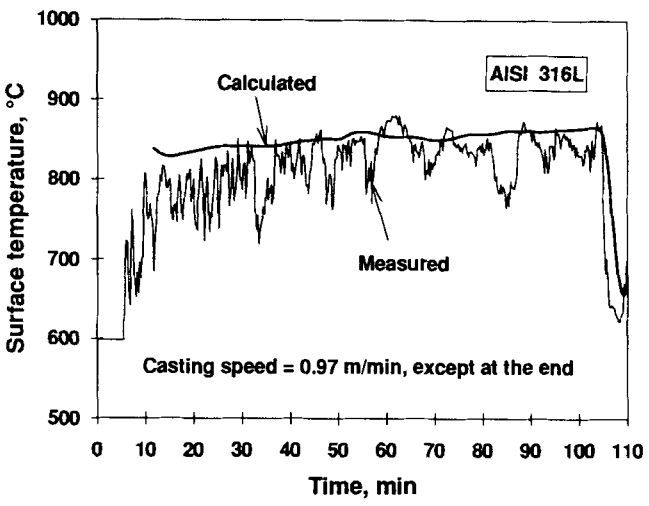

Fig. 13—Comparison between calculated and measured surface temperatures for the steel grade AISI 316L. The comparison point is 5.8 m below the mold on the bottom side.

The presented equations for h_i (Eqs. [23] through [25]) are derived from measurements with $W = 15 - 50$ l/m^2 min. Outside this range, the equations were estimated from the literature.

IX. DISCUSSION

Good agreement between the calculated and measured surface temperatures was obtained, as Figures 11 through 13 show. However, in some cases, the calculated slab surface temperatures were higher than the measurements for approximately 10 to 30 minutes after the start of the cast, as seen in Figure 13. A probable reason for this is that the casting machine rolls and spray cooling water heat up to a steady state condition after start-up. This phenomenon was not taken into account in the model, but it is now being incorporated into the model. The shell thickness was not compared with experimental values. Some experimental shell thickness measurements have recently been carried out, and the analysis of them is currently in progress.

The heat-transfer coefficient depends also on the degree of the oxidation on the surface.[26,40,41] In this study, three different steel grades (AISI 304L, AISI 321, AISI 316L) were used, and AISI 321 especially had a different dependence on the heat-transfer coefficient than the other two grades. AISI 321 is Ti-stabilized and was cast with different casting powder than the other two grades. The correlation between the cooling conditions and the heat-transfer coefficient must be determined separately for each steel group.

There were also situations where the use of an average heat-transfer coefficient for the cooling zones was not accurate enough. For instance, when the casting speed is zero, the same areas of the slab are sprayed by the cooling water while the unsprayed areas may reheat. Such a period cannot be simulated very accurately using average heat-transfer coefficients for the cooling zones. In such cases, the heat-transfer coefficients should be determined within the cooling zones locally more precisely.[7-10]

The aim of the present work was to develop a model which calculates the strand surface temperature profile and the shell thickness profile in the middle region of the strand on-line for process control purposes.

In summary, it can be said that the model gives reliable results if the boundary conditions are correctly determined. It also fulfills the requirements for on-line use. As to the future work, the main aim is to study more precisely the dependence of the heat-transfer coefficient on the cooling conditions (water spray, air mist cooling, steel grade, *etc.*) using both pyrometer and thermoelement measurements. Another aim for future work is the development of on-line applications of the model as a control of the secondary cooling, on-line quality prediction, or optimization of the casting speed. The model is now implemented on a one slab casting machine.

X. CONCLUSIONS

A real-time heat-transfer model for continuous slab casting is presented. The model calculates the strand temperatures and the solid shell thickness profile along the machine as a function of the actual casting variables, strand geometry, and steel grade. The model was tested by carrying out industrial trials, and quite a good agreement between the calculated and measured results was obtained. The model also seems to fulfill the speed requirements concerning its on-line use. A special procedure to determine the boundary conditions for the secondary cooling zones from temperature measurements is also developed and presented.

ACKNOWLEDGMENTS

The authors wish to thank Professor Lauri Holappa at the Helsinki University of Technology and the Technology Development Center for financial support.

REFERENCES

1. J.K. Brimacombe, P.K. Agarwal, L.A. Baptista, S. Hibbins, and B. Prabhakar: In *Proc. 63rd National Open Hearth and Basic*

Oxygen Steel Conf., Washington, Mar. 23–26, 1980, appeared in *Proc. AIME*, vol. 63, pp. 235-52.
2. B. Rogberg: *Scand. J. Metall.*, 1983, vol. 12, pp. 13-21.
3. L. Holappa, E. Laitinen, S. Louhenkilpi, and P. Neittaanmäki: In *Proc. of 24th Annual Conf. of Metallurgists*, The Metallurgical Society of CIM, Vancouver, Canada, 1985, pp. 242-59.
4. V.A. Wills and D.G. McCartney: *Mater. Sci. Technol.*, 1992, vol. 8, pp. 114-22.
5. K.-H. Tache: *Int. J. Numer. Methods Eng.*, 1985, vol. 21, pp. 543-54.
6. K. Kawakami, T. Kitagawa, K. Murakami, Y. Miyashita, Y. Tsuchida, and T. Kawawa: *Nippon Kokan Tech. Rep.*, 1982, No. 36, pp. 26-41.
7. K. Thompson and M. Wolf: *Concost Technol. News*, 1988, vol. 27, p. 6.
8. S. Kojima, T. Matsukawa, and M. Kodama: In *Steelmaking Proc. of the Iron and Steel Society*, Pittsburgh, PA, 1982, pp. 255-62.
9. M. Onishi, T. Ueda, Y. Shinjo, H. Mizata, M. Yao, and T. Fujimura: *Kawasaki Steel Tech. Rep.*, 1981, No. 3, pp. 13-25.
10. K. Okamura and H. Kawashima: *The Sumitomo Search*, 1991, No. 45, pp. 9-16.
11. J.E. Lait, J.K. Brimacombe, and F. Weinberg: *Ironmaking and Steelmaking*, 1974, vol. 1, pp. 90-97.
12. J. Yamasaki, S. Miyahara, M. Kodama, T. Matsukawa, J. Matsuno, and K. Suzuki: in *Proc. of IFAC Control Science and Technology*, Kyoto, Japan, 1981, H. Akashi, ed., Pergamon, Oxford, 1982, pp. 2639-43.
13. M. Bamberger and B. Prinz: *Z. Metall.*, 1986, vol. 77, pp. 234-38.
14. B.I. Krasnov, D.P. Evteev, M.I. Lebedeva, Yu. M. Tsier, and A.V. Skolobanov: *Steel USSR*, 1980, vol. 10, pp. 75-77.
15. P.J. Flint: In *Proc. of 9th Process Technology, 73rd Steelmaking Conf.*, Detroit, MI, 1990.
16. E. Laitinen, S. Louhenkilpi, T. Männikkö, and P. Neittaanmäki: In *Proc. of the 4th Ann. Conf. of the European Consortium for Mathematics in Industry (ECMI)*, St. Wolfgang, Austria, May 29–June 2, 1989, Hansjorg Wacker and Walter Zulehner Teubner, eds., Stuttgart, 1991, pp. 109-21.
17. S. Barozzi, P. Fontana, and P. Pragliola: *Iron Steel Eng.*, 1986, vol. 63, pp. 21-26.
18. K. Okuno, H. Naruwa, T. Kuribayashi, and T. Takamoto: *Iron Steel Eng.*, 1987, vol. 64, pp. 34-38.
19. T. Takawa, R. Takahashi, and M. Tatsuwaki: *The Sumitomo Search*, 1987, May, No. 34, pp. 79-87.
20. S. Kawasaki, H. Arita, M. Kikunaga, Y. Chida, and Z. Kajita: *Nippon Steel Tech. Rep.*, 1984, No. 23, pp. 69-76.
21. K.-H. Spitzer, K. Harste, B. Weber, P. Monheim, and K. Schwerdtfeger: *ISIJ Int.*, 1992, vol. 32, pp. 848-56.
22. E.A. Mizikar: *Trans TMS-AIME*, 1967, vol. 239, pp. 1747-53.
23. I. Saucedo, J. Beech, and G.J. Davies: *Met. Technol.*, 1982, vol. 9, pp. 282-91.
24. R.B. Mahapatra, J.K. Brimacombe, I. Samarasekera, E.F. Paterson, and J.D. Young: In *Proc. of 4th Int. Conf. on Continuous Casting*, Bryssel, Belgium, 1988, Verlag Stahleisen mbH, Düsseldorf, 1988, pp. 655-67.
25. Y. Nishida, W. Droste, and S. Engler: *Metall. Trans B*, 1986, vol. 17B, pp. 833-44.
26. H. Jacobi, G. Kaestle, and K. Wünnenberg: *Ironmaking and Steelmaking*, 1984, vol. 11, pp. 132-45.
27. A. Etienne and B. Mairy: *CRM*, 1979, No. 55, pp. 1-11.
28. J.K. Brimacombe, P.K. Agarwal, S. Hibbins, B. Prabhaker, and L.A. Baptista: *Continuous Casting*, AIME, New York, NY, 1984, vol. 2.
29. N. Kikuchi: *Finite Element Methods in Mechanics*, Cambridge University Press, Cambridge, United Kingdom, 1986.
30. A. Brooks and T.J.R. Hughes: *Comput. Methods Appl. Mech. Eng.*, 1982, vol. 32, pp. 199-259.
31. S.V. Patankar: *Numerical Heat Transfer and Fluid Flow*, Hemisphere Publishing Corporation, Washington, 1980.
32. E. Laitinen and P. Neittaanmäki: *J. Eng. Math.*, 1988, vol. 22, pp. 335-54.
33. E. Laitinen: Ph.D. Thesis, University of Jyväskylä, Jyväskylä, Finland, 1989.
34. M. Křižek and P. Neittaanmäki: *Finite Element Approximation of Variational Problems and Applications*, Longman Scientific and Technical, Longman Group UK Limited, Essex, United Kingdom, 1990.
35. Joel M. Crichlow: *An Introduction to Distributed and Parallel Computing*, Prentice-Hall International (UK) Ltd., 1988.
36. F. Richter: *Die Wichtigsten Physikalischen Eigenschaften von 52 Eisenwerkstoffen*, Verlag Stahleisen M.B.H., Düsseldorf, 1973.
37. T. Ashworth and D.R. Smith: *Therm. Conduct.*, 1985, No. 18, pp. 175-85.
38. A. Goldsmith, T.E. Waterman, and H.J. Hirschhorn: *Handbook of Thermophysical Properties of Solid Material, vol. II: ALLOYS*, The Macmillan Company, New York, NY, 1961.
39. J. Miettinen: *Metall. Trans. A*, 1992, vol. 23A, pp. 1155-70.
40. C. Khler, R. Jeschar, R. Scholz, J. Slowik, and G. Borchardt: *Steel Res.*, 1990, vol. 61, pp. 295-301.
41. J. Slowik, G. Borchardt, C. Khler, R. Jeschar, and R. Scholz: *Steel Res.*, 1990, vol. 61, pp. 302-11.